Chapter 15
Adsorption Microcalorimetry, IR Spectroscopy and Molecular Modelling in Surface Studies

Vera Bolis

Abstract The advantage in coupling adsorption microcalorimetry with IR spectroscopy and/or *ab initio* modelling in surface studies is illustrated by a selection of examples dealing with metal oxides and silica-based (either non porous or microporous) materials. Correlations between thermodynamic and vibrational parameters are illustrated for the adsorption of CO and of NH_3, employed as probe molecules for studying the Lewis/Brønsted acidity of the investigated materials. Surface reconstruction processes, responsible for endothermic effects, are invoked to interpret the unexpectedly low heat measured in the calorimetric cell for the high-coverage adsorption of CO on transition aluminas, the adsorption of NH_3 on a defective all-silica zeolite and the adsorption of H_2O on an amorphous alumino-silicate.

15.1 Introduction

Heat evolved when (reactive) molecules contact the surface of a solid material is related to the molecule/surface site bonding energy. By processing the overall set of volumetric-calorimetric data at increasing equilibrium pressure, both magnitude of the enthalpy of adsorption and its evolution with increasing coverage are obtained. In such a way the possible heterogeneity of the surface (structural, chemical and/or induced) is quantitatively described.

The volumetric-calorimetric data obtained by a Tian-Calvet heat-flow microcalorimeter connected to a gas-volumetric apparatus (as the one described in Chap. 1) being intrinsically molar quantities, their molecular interpretation often requires a multi-techniques approach.

V. Bolis (✉)
Dipartimento di Chimica and NIS Centre of Excellence, Università di Torino,
Via Pietro Giuria 7, 10125 Torino, Italy
e-mail: vera.bolis@gmail.com

A. Auroux (ed.), *Calorimetry and Thermal Methods in Catalysis*,
Springer Series in Materials Science 154, DOI: 10.1007/978-3-642-11954-5_15,

Adsorption microcalorimetry is suitably and fruitfully coupled with complementary techniques, in particular with the ones which are intrinsically apt to detect the nature of both the pristine surface sites and the new terminations created by the chemical interaction of the (probe) molecules with the surface sites [1–3]. IR spectroscopy is an ideal technique for this purpose [4, 5]. On the other hand, the increasing amount of computational *ab initio* results on adspecies formed at simulated model sites is ideally suited to be compared with experimental data from microcalorimetry [6–10].

IR spectroscopy experiments and/or *ab initio* calculations being strategically planned and performed in parallel with the microcalorimetric measurements allow to describe the surface features of a solid material in an almost exhaustive way (nature/structure, population and strength of the surface sites) [11–13].

The combined use of adsorption microcalorimetry, IR spectroscopy and/or *ab initio* calculations will be illustrated for a selection of non-dissociative chemical adsorption cases. In the reported examples, no new surface terminations were originated during the adsorption: only a perturbation of the vibrational features of the adsorptive when adsorbed at the surface was so detected by IR spectroscopy. The experimental details of the microcalorimetric measurements, including the description of the investigated materials, were reported in Chap. 1.

15.2 CO Adsorbed on Coordinatively Unsaturated Metal Cations

The adsorption of carbon monoxide has been widely used over the years in studies aimed at characterizing the surface acidity of coordinatively unsaturated (*cus*) Me^{n+} cations. The *cus* metal cations, either exposed at the dehydrated surface of oxidic materials or located within the dehydrated zeolite nanocavities as charge-balancing cations, are known to act as Lewis acidic sites of variable strength [14].

On non d/d^0 *cus* metal cations, for which any d-electrons π-back-donation is prevented, CO is either simply polarized by the local electric field generated by the positive charge of the *cus* metal cation, or is σ-coordinated to the *cus* metal cation through the C – end lone pair [1–15]. In the former case weak electrostatic adducts, in the latter case reversible chemisorbed species of variable stability are formed. In both electrostatic and σ-coordinated adducts, the C–O stretching frequency of the adsorbed molecule is upwards shifted with respect to the stretching frequency of the free molecule in the gas phase ($\nu_{CO\,ads} > \nu_{CO\,gas} = 2143\,cm^{-1}$). It has been observed that the extent of the C–O stretching frequency shift, defined as $\Delta\nu_{CO} = \nu_{CO\,ads} - \nu_{CO\,gas}$, is a measure of the extent of the lone pair donation to the *cus* cations and so of their electron-accepting properties [16–18]. In this respect, $\Delta\nu_{CO}$ can be taken as a measure of the acidic strength of the *cus* cations, and is correlated to the enthalpy of adsorption, which directly measures the strength of the $Me^{n+} \leftarrow CO$ bond [4, 15, 19–21].

In the case of d-block *cus* metal cations, the strength of the σ-coordinative bond in the carbonyl-like species is reinforced by the π-back donation of d electrons. The actual spectral position of the ν_{CO} band turns out to be a compromise between the upward shift due to the polarization/σ-coordination and the downwards shift due to the π-back donation [1, 22]. As a consequence, the stretching frequency of adsorbed CO can arrive to suffer a downwards shift with respect to the free molecule ($\nu_{COads} < \nu_{COgas}$).

In Fig. 15.1 the possible *cus* metal cation/CO interactions are schematically illustrated. In Fig. 15.1a the plain electrostatic polarization/σ-coordination of the molecule on non d/d^0 *cus* metal cations, implying an upwards shift of the C–O stretching frequency with respect to the free molecule, is reported. In Fig. 15.1b the σ-coordination + π-back donation on d-block *cus* metal cations, for which the C − O stretching frequency can be either slightly upward shifted or downward shifted with respect to the free molecule, according to the weight of the π-back donation contribution with respect to the electrostatic/σ-coordination contribution.

In Fig. 15.2 the shift of the CO stretching frequency ($\Delta\nu_{co}$) is reported as a function of the negative enthalpy of adsorption ($-\Delta_a H$) for CO adsorbed on *cus* Me^{n+} cations (either non d, d^0 or d in nature). The reported plot summarizes a large number of experimental data. $\Delta\nu_{co}$ and $-\Delta_a H$ values were obtained through parallel experiments carried out in different laboratories (see ref. [1] for details on the samples and on the experimental conditions). The reported data will be discussed for CO adsorbed at vanishing coverage on: (i) non-d/d^0 metal cations (circle), (ii) copper and silver metal carbonyls (square and diamonds, respectively), and for CO adsorbed at high coverage on: (iii) transition catalytic alumina (star). Note that series (i) includes also a d^{10} metal cation (*cus* Zn^{2+}) which was found to behave similarly to the non-d metal cations, both when hosted in Y-zeolite cages or when exposed at the surface of dehydrated ZnO [23].

As far as non-d/d^0 metal cations are concerned, a linear correlation between the spectroscopic and thermodynamic quantities does exist (left-top side of the figure), resulting in the Eq. 15.1:

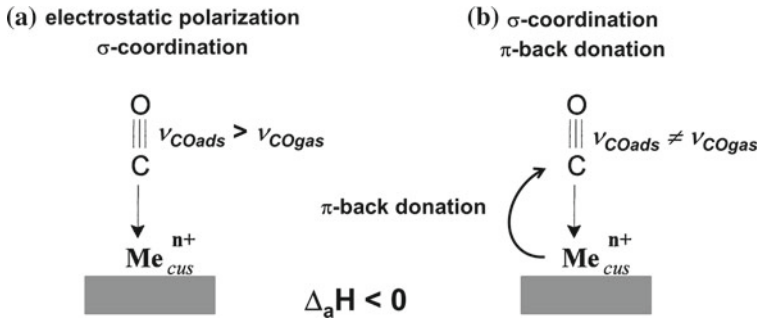

Fig. 15.1 The possible *cus* metal cation/CO interactions are schematically illustrated. **a** electrostatic polarization/σ-coordination (non d/d^0 metal cations); **b** σ-coordination + π-back donation of d electrons (d-block metal cations)

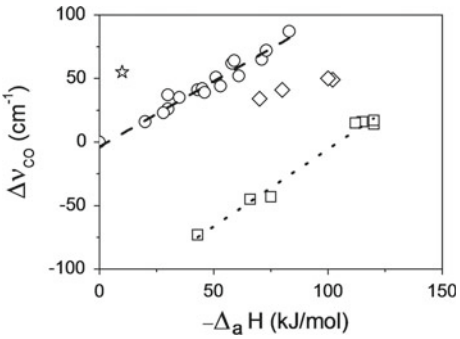

Fig. 15.2 $\Delta\nu_{co}$ *versus* $-\Delta_a H$ for CO adsorbed at vanishing coverage on *cus* metal cations exposed at the surface of either microporous or non-porous dehydrated systems (see Table 3 in ref. [1] for details). *Circle* non-d/d^0 metal cations; *square* Cu-carbonyls; *diamond* Ag-carbonyls; *star* high CO coverage on transition catalytic alumina. Adapted from ref. [1] Fig. 6

$$\Delta\nu_{CO} = \left[(1.03 \pm 0.05)\,\mathrm{cm}^{-1}\,\mathrm{mol}\,(\mathrm{kJ})^{-1}\right]|\Delta_a H| + (-4 \pm 3)\,\mathrm{cm}^{-1} \qquad (15.1)$$

with $R = 0.981$ [1]. The observed linearity for non-d/d^0 metal cations in Fig. 15.2 arises from a statistically significant number of pairs of experimental data, so that Eq. 15.1 can be considered as an empirical rule of general validity for all non-d/d^0 CO complexes.

In the case of d-block metal cations, a lack of correlation with the Eq. 15.1 empirical rule is expected as a consequence of the π-back donation of d-electrons. It was already mentioned that the presence of a π-back-donation contribution does reinforce the strength of the carbonyl bond and does cause a downwards shift of the stretching frequency [22, 24, 25]. This was confirmed by plotting the pairs of IR spectroscopic and microcalorimetric data for Cu- and Ag-carbonyls formed either within the zeolite nanopores or at the surface of metal oxides. The reinforcement of the carbonyl bond was witnessed by: (i) the large heat of adsorption ($q_0 > 100\,\mathrm{kJ\ mol}^{-1}$) measured for both for Cu- and Ag- carbonyls (see Chap. 1, Fig. 1.14) and (ii) the partial irreversibility of the adsorption upon evacuation of pressure (see Chap. 1, Figs. 1.10 and 1.11).

A deviation from the non-d/d^0 metal cations linear plot was clearly observed for both copper and silver species, with remarkable differences between the two *group 11* metals. The increase of $-\Delta_a H$ values for both Cu- and Ag- carbonyls with respect to the non-d/d^0 metal cations adspecies was not accompanied by a correspondent increase of the upwards shift of the C − O stretching frequency.

The formation of well-defined $[\mathrm{Cu\ (CO)}]^+$ complexes within the zeolite nanopores was characterized by $(-\Delta_a H)_0 \approx 120\,\mathrm{kJ\ mol}^{-1}$ and $(\Delta\nu_{co})$ comprised in the 16–14 cm^{-1} range, according to different authors [1, 26]. These pairs of values well agreed with those obtained for CO adsorbed on $Cu/SiO_2{\cdot}Al_2O_3$ ($-\Delta_a H = 115 - 112\,\mathrm{kJ\ mol}^{-1}$ and $\Delta\nu_{co} = 16 - 15\,\mathrm{cm}^{-1}$), as reported in ref. [27].

The low-enthalpy values for Cu-carbonyls reported in Fig. 15.2 refer to $\Delta\nu_{co}$ and $-\Delta_a H$ pairs obtained for partially reduced Cu- species. In one case CO was

adsorbed on a Cu(I)-MFI specimen, in which Cu(I) sites were already engaged with NH_3 ligands, so yielding a mixed amino-carbonyl $[Cu\,(NH_3)\,CO]^+$ complex as illustrated in ref. [1]. The zero-coverage enthalpy change of ≈80 kJ mol^{-1} indicated a weakening of the CO/$\left[Cu\,(NH_3)_n\right]^+$ interaction with respect to the CO/Cu(I) one. The CO stretching frequency for the amino-carbonyl complex was negative ($\Delta\nu_{co} = -43\,cm^{-1}$), confirming the major change in the amino complex Cu/CO interaction with respect to that of the bare Cu(I) cations. In fact, the actual charge density of copper cations in $\left[Cu\,(NH_3)_n\right]^+$ was much lower than that of the pristine *cus* Cu(I) cations, owing to the presence of the charge-releasing NH_3 ligands. This was clearly demonstrated by XANES spectroscopy, as reported in ref. [1, 28]. In the other reported cases, CO was adsorbed on Cu-species grafted on a non-porous ZnO matrix. Cu- species were reduced by thermal treatments in H_2, either partially in the Cu(δ+)/ZnO sample or totally in the Cu(0)/ZnO one, as reported in ref. [29]. For both partially and totally reduced Cu- species, the stretching frequency shift was negative ($\Delta\nu_{co} = -45$ and $-74\,cm^{-1}$, respectively) and the enthalpy change was significantly lower ($-\Delta_a H$ ≈66 and 43 kJ mol^{-1}, respectively) than that for copper sites located within the zeolite nanocavities, and characterized by a well-defined oxidation state of the metal.

By plotting $\Delta\nu_{co}$ against $-\Delta_a H$ values for the adsorption of CO on the various Cu-sites, as illustrated in Fig. 15.2, it is rather evident that the spectroscopic and thermodynamic parameters are once more linearly correlated, as witnessed by the Eq. 15.2:

$$\Delta\nu_{CO} = \left[(1.21 \pm 0.07)\,cm^{-1}mol\,(kJ)^{-1}\right]|\Delta_a H| + (-127 \pm 6)\,cm^{-1} \quad (15.2)$$

with R = 0.993 [1]. The linear decrease of $\Delta\nu_{co}$ with decreasing $-\Delta_a H$ by moving from $\left[Cu\,(CO)_2\right]^+$ to $\left[Cu\,(NH_3)_n\,(CO)\right]^+$ complexes, and down to both Cu(δ+)/ZnO and Cu(0)/ZnO species was interpreted as due to the decrease of the actual charge of copper cations which brought about a progressive extinguishment of the carbonyl bond electrostatic component. This result strongly suggests the major role played by the electrostatic component in the carbonyl-like bonds.

By the inspection of Ag/CO data reported in Fig. 15.2, it is rather evident that the deviation from the Eq. 15.1 empirical line for Ag-carbonyls was not as large as for Cu- carbonyls. This datum indicates that the π-back-donation contribution was lower for the former than for the latter. In fact, the zero-coverage enthalpy of formation for Ag(I)-carbonyl (≈100 kJ mol^{-1}) was lower than for Cu(I)-carbonyl (≈120 kJ mol^{-1}), as reported in ref. [1] and pointed out in Chap. 1 Fig. 1.14. As for the stretching frequency shift, the upwards shift measured for Ag(I)-carbonyls was $\Delta\nu_{co} = 50\,cm^{-1}$, much larger than that measured for Cu(I)-carbonyls ($16 - 14\,cm^{-1}$), confirming the π-back donation minor contribution in the Ag/CO bond. Data for CO adsorbed on Ag(I) sites dispersed at the $SiO_2{\cdot}Al_2O_3$ surface were in fairly good agreement with those for Ag(I)-MFI, as it was reported in ref. [27]. Conversely, a lower enthalpy change was measured for Ag sites characterized by silver species in a not-well defined oxidation state, either hosted within a zeo-

lite nanopores ($\approx$80 kJ mol^{-1}) or dispersed at the SiO_2 surface ($\approx$70 kJ mol^{-1}). The correspondent stretching frequency shift ($\Delta\nu_{CO} = 34\,cm^{-1}$ for the former and 41 cm^{-1} for the latter) was lower than for Ag(I)-MFI (50 cm^{-1}) [27].

In the silver case, owing to the limited set of partially reduced Ag-carbonyls data, it was not possible to draw any reasonable correlation. A clear trend was however observed: once more as far as the electrostatic component contribution decreases, as a consequence of the reduced actual charge of the metal cation, the strength of the interaction decreases.

By a further inspection of Fig. 15.2, it turns out that the pair of $-\Delta_a H$ and $\Delta\nu_{co}$ values for CO adsorbed on transition catalytic aluminas is definitely out of the Eq. 15.1 correlation line, if the high coverage values are considered.

In fact, the pairs of values for CO adsorbed at low coverage on both $\gamma-$ and $\delta,\theta-Al_2O_3$ were found to fit quite well with the Eq. 15.1 correlation plot: $\Delta\nu_{CO} = 60-70\,cm^{-1}$ and $-\Delta_a H \approx 60-70$ kJ mol^{-1}. Conversely, at high CO coverage the measured heat was surprisingly low ($-\Delta_a H \approx 10$ kJ mol^{-1}) with respect to the vibrational parameter ($\Delta\nu_{CO} = 55$ cm^{-1}).

It is here recalled that in cation-deficient spinel transition aluminas, the Al(III) cations are located either in tetrahedral or octahedral cavities of the cubic close packed array of oxide ions [15, 30]. In the $\gamma-$ and $\delta,\theta-Al_2O_3$ here discussed, two CO adspecies were formed at the surface when outgassed at $T = 773$ K. The two adspecies were defined as $(CO)_A$ and $(CO)_B$ in refs. [15, 31], being their presence witnessed by the appearance of ν_{CO} bands at $\approx$2205 and 2215 cm^{-1}, respectively. A third CO adspecies defined as $(CO)_C$, witnessed by the appearance of a ν_{CO} band at $\approx 2230\,cm^{-1}$, was observed only when the surface was outgassed at $T = 1023$ K [15]. The formation of more than one CO adspecies was ascribed to the presence of the tetrahedral *cus* Al(III) cations located in different crystallographic positions. The tetrahedral *cus* Al(III) cations are in fact known to be the only sites able to adsorb at room temperature, being the octahedral *cus* ones too weakly acidic to do so [4, 30, 31]. The vanishing coverage enthalpy of formation of the three species ($-\Delta_a H \approx 58$, 73 and 83 kJ mol^{-1} for $(CO)_A$, $(CO)_B$ and $(CO)_C$, respectively) was found correlated with the correspondent shift: 62, 72 and 87 cm^{-1} for $(CO)_A$, $(CO)_B$ and $(CO)_C$, respectively) as reported in refs. [1, 15].

In Fig. 15.3 the heats of adsorption for γ- and $\delta,\theta-Al_2O_3$, both activated at $T = 773$ K, are reported as a function of CO uptake in comparison with the correspondent data for TiO_2-anatase (activated at $T = 673$ K). The zero-coverage heat of CO adsorption on γ- and $\delta,\theta-Al_2O_3$ ($\approx$60 kJ mol^{-1}) was close to the value measured for CO adsorbed on *cus* Ti(IV) cations on TiO_2 [20] and was compatible with a plain electrostatic polarization/σ-coordination of CO at the Lewis acidic AI(III) sites [4, 32]. However, remarkable differences were observed between the titania and alumina plots as far as the surface coverage increased. The heat of adsorption on TiO_2 decreased only slightly upon increasing coverage, whereas on Al_2O_3 (both $\gamma-$ and δ,θ-phases) the heat values dropped abruptly down to very low values ($q \approx 10$ kJ mol^{-1}, at the highest coverage reached at $p_{CO} \approx 80$ *Torr*).

The assignment of this surprisingly low heat value to the adsorption of CO on Lewis acidic sites other than the tetrahedral Al(III) cations was discarded by the IR

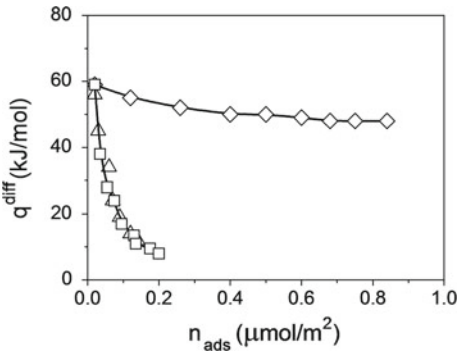

Fig. 15.3 Differential heat of adsorption (at $T = 303\,\mathrm{K}$) as a function of the increasing CO uptake on: TiO_2-anatase pre-outgassed at $T = 673\,\mathrm{K}$ (*diamond*); $\gamma-Al_2O_3$ (*triangle*) and $\delta,\theta-Al_2O_3$ (*square*), both pre-outgassed at $T = 773\,\mathrm{K}$. Adapted from ref. [4] Fig. 3b

spectra which confirmed the presence of the sole σ-coordination of CO, through the C-end, on the Lewis acidic tetrahedral Al(III) sites [4, 15, 30, 31].

A process other than a plain σ-coordination taking place at the Al_2O_3/CO interface was invoked to justify the lack of correlation with the linear plot described by Eq. 15.1 for the high-coverage $-\Delta_a H$ value. It was demonstrated that the heat measured at high coverage comprised two different processes: (i) the exothermic σ-coordination of CO on tetrahedral *cus* Al(III) cations, and (ii) an endothermic surface reconstruction accompanying the adsorption process. In this respect, it is here recalled that the overall heat measured within the calorimetric cell is irrespective of how many and what kind of processes are actually occurring at the gas–solid interface.

In Fig. 15.4a , the presence of surface Al(III) cations engaged with strained Al–O bonds (and so not available as such for the interaction with molecules) is schematically illustrated [4, 30]. The adsorption of on this kind of Al(III) cations, which causes the O–Al groups interaction to be broken, is schematically illustrated in Fig. 15.4b. This effect was in fact evidenced at high coverage of CO by IR spectroscopy in the region of the Al–O modes (1100–1000 cm^{-1}), and was found to be entirely reversible [4, 30, 31, 33].

The modification of the surface structure produced by the rupture of the Al$\cdots$O–Al moieties interaction is intrinsically endothermic, and caused the measured heat for the Al_2O_3/CO interaction to be lower than what expected for a plain σ-coordination. This result does justify the dramatically low heat of interaction measured within the calorimetric cell, and does explain the lack of correlation between the energetic and vibrational parameters [1, 20, 34, 35].

In conclusion, in transition aluminas only the zero-coverage heat of adsorption, which is correlated to the shift of the stretching frequency, can be taken as a measure of the electron accepting properties of *cus* Al(III) cations and of the strength of the σ-dative bonds formed.

The lack of correlation between thermodynamic and spectroscopic data for CO adsorbed on transition aluminas revealed that the interaction at the gas-solid interface

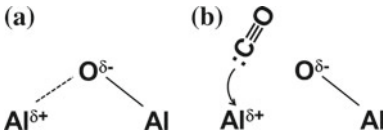

Fig. 15.4 **a** Surface Al(III) cations engaged with strained Al–O bonds in transition aluminas; **b** the adsorption of CO on the engaged Al(III) cations causes the Al(III)/O–Al interaction to be broken

is more complicated than expected. Also in this respect, the joint use of adsorption microcalorimetry and IR spectroscopy was proved very useful in arriving at a detailed molecular interpretation of the process.

15.3 NH_3 Adsorbed on All-Silica MFI Zeolites (Silicalite)

Defective Silicalite is an all-silica MFI zeolite, which is non-hydrophobic and weakly acidic as a consequence of the abundant polar defects (Si–OH nests) generated by the structure to compensate the Si atoms vacancies [7]. IR spectra in the ν_{OH} stretching frequency region give a clear evidence of the presence of Si–OH nests, which are characterized by a different geometrical arrangement according to the synthesis procedure and/or post-synthesis treatments, as illustrated in ref. [36].

The shift of the stretching frequency of the Si–OH terminations ($\Delta\nu_{OH}$) when the latter are engaged in H-bonding interaction with molecules is generally taken as a measure of the strength of the H-bonding interaction [6, 13, 37–39]. In the case of NH_3 adsorbed on a variety of silica–based materials (defective MFI-Silicalite and amorphous non-porous silica) $\Delta\nu_{OH}$ was found to be linearly correlated to the zero-coverage adsorption enthalpy $(-\Delta_a H)_0$, as illustrated in Fig. 15.5. See ref. [36] for details on the samples, and see also Chap. 1 Fig. 1.15b for the differential heat versus coverage plots of the MFI-Silicalite investigated specimens.

The pair of $\Delta\nu_{OH}$ and $(-\Delta_a H)_0$ values measured for one of the investigated MFI-Silicalite samples (Sil-B, see Chap. 1 Fig. 1.15b) was found to deviate from the linear correlation illustrated in the plot. The zero-coverage adsorption enthalpy for Sil-B

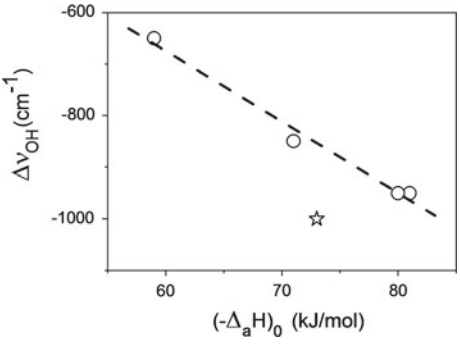

Fig. 15.5 Shift of the ν_{OH} stretching frequency ($\Delta\nu_{OH}$) versus the zero-coverage adsorption enthalpy $(-\Delta_a H)_0$ measured for NH_3 on a variety of silica–based materials (defective MFI-Silicalite and amorphous non-porous silica). Adapted from ref. [36] Fig. 6

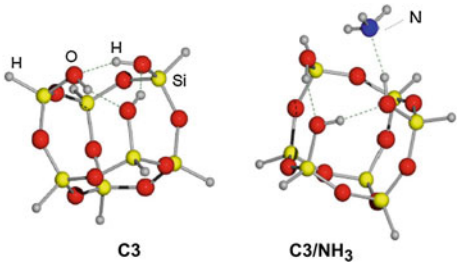

Fig. 15.6 Cluster model of a secondary building unit of MFI-Silicalite simulating a Si–OH nest arranged in a closed chain (ring), either free (C3) or in H-bonding interaction with one NH_3 molecule ($C3/NH_3$). Geometries were fully optimized without constraints at B3-LYP/6-31+G(d,p) level. Atomic symbols for cluster atoms are reported in C3 model; atomic symbol for ammonia N atom on $C3/NH_3$ model. Adapted from ref. [36] Fig. 8

($\approx$73 kJ mol^{-1}) was lower than that expected on the basis of the $\Delta_{\nu_{CO}}$ value ($\approx$85 kJ mol^{-1}). It is here recalled that the heat released for the adsorption of NH_3 on Sil-B was lower than for the other investigated samples in the whole coverage examined (see curve 3 in Chap. 1 Fig. 1.15).

Also in this case, the apparently anomalous behavior of one sample was interpreted as an indication of the presence of phenomena others than a plain adsorption. In fact, the adsorption of NH_3 on Sil-B was demonstrated to imply an endothermic step which lowered the measured heat value.

The Sil-B sample was characterized by a structured spectroscopic response in the ν_{OH} region. The peculiar structure of the ν_{OH} band of this specimen was interpreted as due to the presence of small highly structured rings of mutually interacting silanol groups located within the nanopores of the zeolite. This was also suggested by neutron diffraction data [40, 41] and was confirmed by an *ab initio* modeling study. A nest arranged in a closed chain (ring) was simulated by a cluster model of a secondary building unit of MFI-Silicalite. The model is reported in Fig. 15.6, either free (C3) or in H-bonding interaction with one molecule ($C3/NH_3$). Geometries were fully optimized without constraints at B3-LYP/6-31+G(d,p) level. The *ab initio* modeling study demonstrated that rings must be first "opened" in order to become available for the interaction with NH_3. The insertion of one molecule in the ring required the breaking of the Si–OH$\cdots$OH–Si mutual H-bonding interaction, the energetic cost of which was computed to be as high as $\approx$12 kJ mol^{-1}. This value turned out to be in fairly good agreement with the experimental difference between the expected ($\approx$85 kJ mol^{-1}) and the measured ($\approx$73 kJ mol^{-1}) enthalpy of adsorption [36].

Also in this case, the accurate interpretation at molecular detail of the volumetric-calorimetric results was achieved thanks to the joint use of microcalorimetry, IR spectroscopy and *ab initio* calculations.

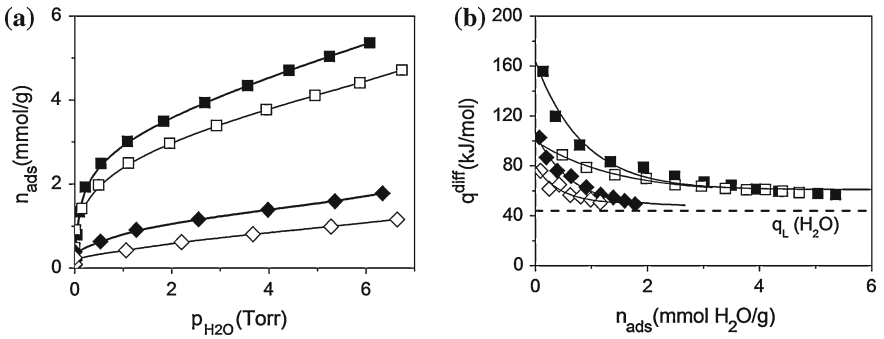

Fig. 15.7 **a** volumetric isotherms, **b** differential heats of adsorption versus coverage plots of H_2O_{vap} adsorbed at $T = 303\,K$ on H-BEA (*square*) and on $SiO_2{\cdot}Al_2O_3$ (*diamond*). H-BEA was pre-outgassed at $T = 873\,K$, $SiO_2{\cdot}Al_2O_3$ at $T = 673\,K$. *Solid symbols* first run; *open symbols* second run of adsorption. Adapted from ref. [7] Fig. 8

15.4 H_2O Vapor Adsorbed on Crystalline and on Amorphous Alumino-Silicates

The adsorption of water on a crystalline zeolite (H-BEA) and on an amorphous alumino-silicate specimen ($SiO_2{\cdot}Al_2O_3$) was studied in order to investigate the nature/structure of the acidic species originated by the presence of Al moieties the silica matrix [7]. It is generally accepted that proton-exchanged zeolites and alumino-silicate materials of similar composition exhibit different acidic features [42]. In particular, it was demonstrated that the Brønsted acidic strength, which is strongly dependent on the structural features of the material, is highest for H-zeolites [43].

In Fig. 15.7, volumetric isotherms (Sect. a) and differential heats (Sect. b) of water vapor (H_2O_{vap}) adsorption for the two investigated specimens are reported. The two samples,[1] were pre-outgassed for 2 h at either $T = 873\,K$ (H-BEA) or $T = 673\,K$ ($SiO_2{\cdot}Al_2O_3$), at a residual pressure $p \leq 10^{-5} Torr$ in order to ensure a maximum density of Lewis and Brønsted acidic sites.

The H – BEA specific adsorption capacity was much larger than that of $SiO_2{\cdot}Al_2O_3$, as witnessed by the volumetric isotherms. For instance at $p = 6\,Torr$, uptake was 5.3 mmol g^{-1} for against only 1.7 mmol g^{-1} for $SiO_2{\cdot}Al_2O_3$. In both cases the adsorption was found to be partially irreversible (2nd run isotherms lie below 1st run isotherms) but the percent of the irreversible component was much larger for $SiO_2{\cdot}Al_2O_3$ than for H-BEA: ≈40 % *versus* ≈20 % of the total uptake, respectively. This datum suggested that H_2O_{vap} adsorption on the amorphous alumino-silicate caused an irreversible modification of the surface larger than on the crystalline specimen.

[1] H-BEA ($\frac{SiO_2}{Al_2O_3} = 4.9$) features are reported in Chap. 1 (Sect. 1.4.1). The amorphous alumino-silicate ($\frac{SiO_2}{Al_2O_3} = 5.8$) was purchased by Strem Chemicals, Inc.

$SiO_2{\cdot}Al_2O_3$ being more reactive towards water than H-BEA, a larger energy of interaction with H_2O_{vap} was expected for the former than for the latter. Surprisingly, the heat of adsorption curves reported in Fig. 15.7b indicate that the heat of adsorption was dramatically larger for the crystalline than for the amorphous alumino-silicate, in the whole range of coverage examined. The zero-coverage heat of adsorption was $\approx$160 kJ mol^{-1} for H-BEA and $\approx$110 kJ mol^{-1} for $SiO_2{\cdot}Al_2O_3$. At high coverage, the former sample heat values lie well above the latent heat of liquefaction of water, $q_L = 44$ kJ mol^{-1}, while the latter sample heat values approach q_L. The same trend was observed for the 2nd run reversible adsorption.

Also in this case, an endothermic step during the adsorption was invoked as a possible explanation for the large $SiO_2{\cdot}Al_2O_3$ surface reactivity surprisingly not accompanied by a high energy of interaction with water. The endothermic step of the overall process was due to the deformation/reconstruction of the surface, consequent to the interaction with water molecules. This process is expected to be facilitated by the flexible structure of the amorphous alumino-silicate and inhibited by the rigidity of the crystalline zeolite framework. In fact, the Lewis acidic *cus* Al(III) atoms, when making part of a rigid zeolite framework, acquire a close similarity with the Lewis acidic sites exposed at the ionic surface of transition aluminas [44]. This was confirmed by the closeness of the zero-coverage heats of adsorption of H_2O_{vap} on $\delta-Al_2O_3$ and H-BEA ($\approx$180 and $\approx$160 kJ mol^{-1}, respectively) [7]. Conversely, the covalent $SiO_2{\cdot}Al_2O_3$ *cus* Al(III) species being exposed at a pliable amorphous $Si-O-Al$ surface were much less available for the interaction with molecules than those making part of the above mentioned rigid structures. As a consequence of the surface reconstruction allowing Al(III) species to interact with water molecules, the measured heat for $SiO_2{\cdot}Al_2O_3$ was lower than what expected for a plain adsorption.

This interpretation was supported by the *ab initio* modeling results described in ref. [7]. Owing to the large uncertainty from the experiments of the local structure around the Al atom, two topological different clusters (LS and LC structures) were designed to simulate the Lewis acidic site, as illustrated in Fig. 15.8, top side row. LS model was adopted to mimic highly strained moieties, typical of defects located in nanocavities. [32] The cluster LC was conversely adopted to simulate the surface species partially saturated by the coordination with an additional nearby framework O atom. This structure can be reasonably assumed as a model for $SiO_2{\cdot}Al_2O_3$,[7] in which the Al atom is allowed to expand its coordination thanks to the flexibility of the Si-O-Al amorphous structure. The structure of all clusters, either free or interacting with water (*vide infra*), were fully optimized at *ab initio* level using the B3-LYP/6-31+G(d,p) model chemistry [32, 45].

In the bottom side row of Fig. 15.8, the B3-LYP/6-31+G(d,p) optimized structures of LS and LC clusters interacting with one molecule (LSW and LCW, respectively) are reported. The computed water binding energies (BE) were corrected for the basis set superposition error, using the standard Boys-Bernardi counterpoise method [46]. It turned out that H_2O interacts much less strongly with LC (BE$-$LCW $\approx$109 kJ mol^{-1}) than with LS (BE$-$LSW $\approx$160 kJ mol^{-1}), in agreement with the lower local coordinative unsaturation of the LC-Al(III) atom with respect to that of the LS model. When H_2O is adsorbed at the LC site, a fraction of

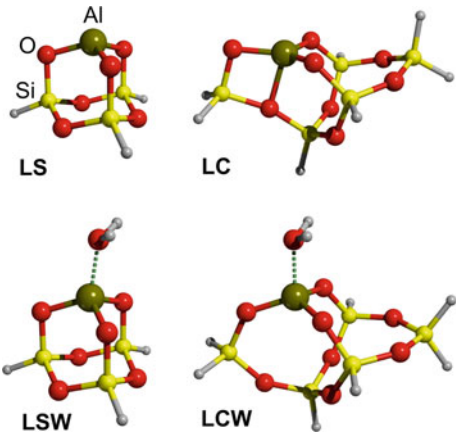

Fig. 15.8 *Top side row* B3-LYP/6-31+G(d,p) optimized clusters mimicking Lewis acidic Al(III) sites. LS model mimics highly strained Al(III)atoms, typical of defects present in H-BEA zeolites; LC cluster simulates the Al(III) atoms coordinating an additional nearby framework O atom. *Bottom side row* B3-LYP/6-31+G(d,p) optimized structures of the LS and LC clusters interacting with one H_2O molecule (LSW and LCW, respectively). Atomic symbols are reported in the model cluster LS. Adapted from ref. [7] Figs. 2 and 3

the adsorption energy is lost to pull out the Al atom from the amorphous framework. Conversely, in the crystalline material the acidic sites are already in place, as imposed by the rigidity of the structure. The "extraction" of the Al-containing site requires an energy cost which was computed to be $\approx 25\,\%$ of the total binding energy for the LCW case [7].

Once more the *ab initio* modeling results allowed to properly interpret the apparently anomalous results obtained by adsorption microcalorimetry, confirming the hypothesis formulated to justify the experimental data.

15.5 Conclusions

A few examples of adsorption processes accompanied by an endothermic step due to the deformation/reconstruction of the surface in interaction with molecules were illustrated. In the reported cases, the heat measured within the calorimetric cell was the combination of an exothermic (adsorption) and an endothermic (surface reconstruction) effect, which caused the calorimetrically measured heat to be lower than what expected on the basis of a plain adsorption. An extra-care in interpreting (at molecular level) the experimental calorimetric results should be addressed in several cases, and in this respect it is quite fruitful to complement the molar volumetric-calorimetric data with results from other approaches, typically the various spectroscopic methods and/or the *ab initio* molecular modeling.

References

1. V. Bolis, A. Barbaglia, S. Bordiga, C. Lamberti, A. Zecchina, Heterogeneous nonclassical carbonyls stabilized in Cu(I)- and Ag(I)-ZSM-5 zeolites: thermodynamic and spectroscopic features. J. Phys. Chem. B **108**(28), 9970–9983 (2004). doi:10.1021/Jp049613e
2. V. Bolis, S. Maggiorini, L. Meda, F. D'Acapito, G.T. Palomino, S. Bordiga, C. Lamberti, X-ray photoelectron spectroscopy and x-ray absorption near edge structure study of copper sites hosted at the internal surface of ZSM-5 zeolite: A comparison with quantitative and energetic data on the CO and NH_3 adsorption. J. Chem. Phys. **113**(20), 9248–9261 (2000). doi:10.1063/1.1319318
3. V. Bolis, S. Bordiga, C. Lamberti, A. Zecchina, A. Carati, F. Rivetti, G. Spano, G. Petrini, Heterogeneity of framework Ti(IV) in Ti-silicalite as revealed by the adsorption of NH_3 Combined calorimetric and spectroscopic study. Langmuir **15**(18), 5753–5764 (1999). doi:10.1021/la981420t
4. V. Bolis, G. Cerrato, G. Magnacca, C. Morterra, Surface acidity of metal oxides. Combined microcalorimetric and IR-spectroscopic studies of variously dehydrated systems. Thermochim Acta **312**, 63–77 (1998)
5. V. Aina, F. Bonino, C. Morterra, M. Miola, C.L. Bianchi, G. Malavasi, M. Marchetti, V. Bolis, Influence of the chemical composition on nature and activity of the surface layer of Zn-substituted Sol-Gel (bioactive) glasses. J. Phys. Chem. C **115**(5), 2196–2210 (2011). doi:10.1021/Jp1101708
6. J. Sauer, P. Ugliengo, E. Garrone, V.R. Saunders, Theoretical-study of Van-Der-Waals complexes at surface sites in comparison with the experiment. Chem. Rev. **94**(7), 2095–2160 (1994). doi:10.1021/cr00031a014
7. V. Bolis, C. Busco, P. Ugliengo, Thermodynamic study of water adsorption in high-silica zeolites. J. Phys. Chem. B **110**(30), 14849–14859 (2006). doi:10.1021/Jp061078q
8. C. Busco, V. Bolis, P. Ugliengo, Masked Lewis sites in proton-exchanged zeolites: a computational and microcalorimetric investigation. J. Phys. Chem. C **111**(15), 5561–5567 (2007). doi:10.1021/Jp0705471
9. M. Corno, C. Busco, V. Bolis, S. Tosoni, P. Ugliengo, Water adsorption on the stoichiometric (001) and (010) surfaces of hydroxyapatite: a periodic B3LYP study. Langmuir **25**(4), 2188–2198 (2009). doi:10.1021/La803253k
10. M. Corno, A. Rimola, V. Bolis, P. Ugliengo, Hydroxyapatite as a key biomaterial: quantum-mechanical simulation of its surfaces in interaction with biomolecules. Phys. Chem. Chem. Phys. **12**(24), 6309–6329 (2010). doi:10.1039/C002146f
11. V. Bolis, C. Busco, V. Aina, C. Morterra, P. Ugliengo, Surface properties of silica-based biomaterials: Ca species at the surface of amorphous silica as model sites. J. Phys. Chem. C **112**(43), 16879–16892 (2008). doi:10.1021/Jp805206z
12. V. Bolis, C. Busco, G. Martra, L. Bertinetti, Y. Sakhno, P. Ugliengo, F. Chiatti, M. Corno, N. Roveri, Coordination chemistry of Ca sites at the surface of nanosized hydroxyapatite: interaction with H_2O and CO. Phil. Trans. R. Soc. a-Math. Phys. Eng. Sci. **370**(1963), 1313–1336 (2012). doi:10.1098/rsta.2011.0273
13. M. Armandi, V. Bolis, B. Bonelli, C.O. Arean, P. Ugliengo, E. Garrone, Silanol-related and unspecific adsorption of molecular ammonia on highly dehydrated silica. J. Phys. Chem. C **115**(47), 23344–23353 (2011). doi:10.1021/Jp206301c
14. K.I. Hadjiivanov, G.N. Vayssilov, Characterization of oxide surfaces and zeolites by carbon monoxide as IR probe molecule. Adv. Catal. **47**, 307–511 (2002). doi:10.1016/S0360-0564(02)47008-3
15. V. Bolis, G. Magnacca, C. Morterra, Surface properties of catalytic aluminas modified by alkaline-earth metal cations: a microcalorimetric and IR-spectroscopic study. Res. Chem. Intermed. **25**(1), 25–56 (1999). doi:10.1163/156856799X00374
16. A. Zecchina, C. Lamberti, S. Bordiga, Surface acidity and basicity: general concepts. Catal. Today **41**(1–3), 169–177 (1998). doi:10.1016/S0920-5861(98)00047-9

17. A.M. Ferrari, P. Ugliengo, E. Garrone, Ab initio study of the adducts of carbon monoxide with alkaline cations. J. Chem. Phys. **105**(10), 4129–4139 (1996). doi:10.1063/1.472283
18. C. Lamberti, S. Bordiga, F. Geobaldo, A. Zecchina, C.O. Arean, Stretching frequencies of cation CO adducts in alkali-metal exchanged zeolites—an elementary electrostatic approach. J. Chem. Phys. **103**(8), 3158–3165 (1995). doi:10.1063/1.470249
19. C. Morterra, E. Garrone, V. Bolis, B. Fubini, An infrared spectroscopic characterization of the coordinative adsorption of carbon-monoxide on TiO_2. Spectrochim. Acta Part A-Mol. Biomol. Spectrosc. **43**(12), 1577–1581 (1987). doi:10.1016/S0584-8539(87)80051-X
20. V. Bolis, B. Fubini, E. Garrone, C. Morterra (1989) Thermodynamic and vibrational characterization of CO adsorption on variously pretreated anatase. J. Chem. Soc. Faraday Trans. I **85**, (1383–1395)
21. E. Garrone, V. Bolis, B. Fubini, C. Morterra, Thermodynamic and spectroscopic characterization of heterogeneity among adsorption sites—CO on anatase at ambient-temperature. Langmuir **5**(4), 892–899 (1989). doi:10.1021/la00088a002
22. A.J. Lupinetti, S.H. Strauss, G. Frenking, Nonclassical metal carbonyls. Prog. Inorg. Chem. **49**, 1–112 (2001). doi:10.1002/9780470166512.ch1
23. V. Bolis, B. Fubini, E. Garrone, E. Giamello, C. Morterra, in *Studies in Surface Science and Catalysis: Structure and Reactivity of Surfaces*, ed. by C. Morterra, A. Zecchina, G. Costa, vol 48 (Elsevier Sci. Publ. B.V., 1989) pp. 159–166
24. S.H. Strauss, Copper(I) and silver(I) carbonyls. To be or not to be nonclassical. J. Chem. Soc. Dalton Trans. **1**, 1–6 (2000). doi:10.1039/a908459b
25. Q. Xu, Metal carbonyl cations: generation, characterization and catalytic application. Coord. Chem. Rev. **231**(1–2), 83–108 (2002). doi:10.1016/S0010-8545(02)00115-7
26. Y. Kuroda, Y. Yoshikawa, R. Kumashiro, M. Nagao, Analysis of active sites on copper ion-exchanged ZSM-5 for CO adsorption through IR and adsorption-heat measurements. J. Phys. Chem. B **101**(33), 6497–6503 (1997). doi:10.1021/jp9710796
27. Y. Kuroda, H. Onishi, T. Mori, Y. Yoshikawa, R. Kumashiro, M. Nagao, H. Kobayashi, Characteristics of silver ions exchanged in ZSM-5-type zeolite, aluminosilicate, and SiO_2 samples: In comparison with the properties of copper ions exchanged in these materials. J. Phys. Chem. B **106**(35), 8976–8987 (2002). doi:10.1021/Jp020507r
28. V. Bolis, S. Bordiga, G.T. Palomino, A. Zecchina, C. Lamberti, Calorimetric and spectroscopic study of the coordinative unsaturation of copper(I) and silver(I) cations in ZSM-5 zeolite - Room temperature adsorption of NH_3. Thermochim. Acta **379**(1–2), 131–145 (2001). doi:10.1016/S0040-6031(01)00612-8
29. E. Giamello, B. Fubini, V. Bolis, Microcalorimetric investigation of the interaction of carbon-monoxide with coprecipitated cupric oxide zinc-oxide catalysts in well-defined oxidation-states. Appl. Catal. **36**(1–2), 287–298 (1988). doi:10.1016/S0166-9834(00)80122-0
30. C. Morterra, G. Magnacca, A case study: surface chemistry and surface structure of catalytic aluminas, as studied by vibrational spectroscopy of adsorbed species. Catal. Today **27**(3–4), 497–532 (1996). doi:10.1016/0920-5861(95)00163-8
31. C. Morterra, V. Bolis, G. Magnacca, IR spectroscopic and microcalorimetric characterization of Lewis-acid sites on (transition phase) Al_2O_3 using adsorbed CO. Langmuir **10**(6), 1812–1824 (1994). doi:10.1021/la00018a033
32. V. Bolis, M. Broyer, A. Barbaglia, C. Busco, G.M. Foddanu, P. Ugliengo, Van der Waals interactions on acidic centres localized in zeolites nanocavities: a calorimetric and computer modeling study. J. Mol. Catal. a Chem. **204**, 561–569 (2003). doi:10.1016/S1381-1169(03)00339-X
33. L. Marchese, S. Bordiga, S. Coluccia, G. Martra, A. Zecchina, Structure of the surface sites of delta-Al_2O_3 as determined by high-resolution transmission electron-microscopy, computer modeling and infrared-spectroscopy of adsorbed CO. J. Chem. Soc. Faraday Trans. 1 Phys. Chem. Condens. Phase **89**(18), 3483–3489 (1993). doi:10.1039/ft9938903483
34. V. Bolis, B. Fubini, E. Garrone, C. Morterra, P. Ugliengo, Induced heterogeneity at the surface of group-4 dioxides as revealed by CO adsorption at room-temperature. J. Chem. Soc. Faraday Trans. **88**(3), 391–398 (1992). doi:10.1039/ft9928800391

35. V. Bolis, C. Morterra, B. Fubini, P. Ugliengo, E. Garrone, Temkin-type model for the description of induced heterogeneity—CO adsorption on group-4 transition-metal dioxides. Langmuir **9**(6), 1521–1528 (1993). doi:10.1021/la00030a017
36. V. Bolis, C. Busco, S. Bordiga, P. Ugliengo, C. Lamberti, A. Zecchina, Calorimetric and IR spectroscopic study of the interaction of NH_3 with variously prepared defective silicalites—comparison with ab initio computational data. Appl. Surf. Sci. **196**(1–4), 56–70 (2002). doi:10.1016/S0169-4332(02)00046-6
37. A. Zecchina, S. Bordiga, G. Spoto, D. Scarano, G. Petrini, G. Leofanti, M. Padovan, C.O. Arean, Low-temperature fourier-transform infrared investigation of the interaction of CO with nanosized ZSM5 and silicalite. J. Chem. Soc. Faraday Trans. **88**(19), 2959–2969 (1992). doi:10.1039/ft9928802959
38. H. Knozinger, *Handbook of Heterogeneous Catalysis*, vol. 2 (Wiley/VCH, Weinheim, 1997)
39. M. Armandi, B. Bonelli, I. Bottero, C.O. Arean, E. Garrone, Thermodynamic features of the reaction of ammonia with the acidic proton of H-ZSM-5 as studied by variable-temperature IR spectroscopy. J. Phys. Chem. C **114**(14), 6658–6662 (2010). doi:10.1021/Jp100799k
40. G. Artioli, C. Lamberti, G.L. Marra, Neutron powder diffraction study of orthorhombic and monoclinic defective silicalite. Acta Crystallogr. Sect. B Struct. Sci. **56**, 2–10 (2000)
41. C. Lamberti, S. Bordiga, A. Zecchina, G. Artioli, G. Marra, G. Spano, Ti location in the MFI framework of Ti-silicalite-1: a neutron powder diffraction study. J. Am. Chem. Soc. **123**(10), 2204–2212 (2001). doi:10.1021/Ja003657t
42. M. Trombetta, G. Busca, S. Rossini, V. Piccoli, U. Cornaro, A. Guercio, R. Catani, R.J. Willey, FT-IR studies on light olefin skeletal isomerization catalysis III. Surface acidity and activity of amorphous and crystalline catalysts belonging to the SiO_2-Al_2O_3 system. J. Catal. **179**(2), 581–596 (1998). doi:10.1006/jcat.1998.2251
43. M.M. Huang, A. Auroux, S. Kaliaguine, Crystallinity dependence of acid site distribution in HA HX and HY zeolites. Microporous Mater. **5**(1–2), 17–27 (1995). doi:10.1016/0927-6513(95)00028-8
44. G. Della Gatta, B. Fubini, L. Stradella, Energies of different surface rehydration processes on "eta", "theta" and "alpha" aluminas. Journal of the Chemical Society. Faraday Trans 2 Mol. Chem. Phys. **73** (7):1040–1049 (1977) doi:10.1039/F29777301040
45. V. Bolis, A. Barbaglia, M. Broyer, C. Busco, B. Civalleri, P. Ugliengo, Entrapping molecules in zeolites nanocavities: a thermodynamic and ab-initio study. Orig. Life Evol. Biosph. **34**(1–2), 69–77 (2004). doi:10.1023/B:ORIG.0000009829.11244.d1
46. S.F. Boys, F. Bernardi, The calculation of small molecular interactions by the differences of separate total energies. Some procedures with reduced errors. Mol. Phys. **19**(4), 553–566 (1970). doi:10.1080/00268977000101561